Theory of Equilibrium Temperatures in Radiative-Turbulent Atmospheres

KUO-NAN LIOU AND SZU-CHENG S. OU

Department of Meteorology, University of Utah, Salt Lake City 84112

(Manuscript received 16 June 1982, in final form 12 October 1982)

ABSTRACT

We have developed a thermodynamic model for the determination of the temperature profile based on the balance of radiative and turbulent fluxes. In the context of a one-dimensional case, we show that the temperature field is governed by a first-order differential-integro equation involving temperature to the fourth power. In conjunction with the temperature profile determination, parameterization programs for the transfer of broadband thermal infrared and solar fluxes in inhomogeneous atmospheres are developed. In addition, the vertical transport is parameterized using a first-order closure scheme with the eddy thermal diffusion coefficients derived either from known theories or from available data. By virtue of an efficient perturbation technique devised for the solution of the thermal equilibrium temperature, we show that the simulated temperatures compare well with those of a standard atmosphere employing climatological water vapor, ozone and cloud profiles. Simulations using the steady-state one-dimensional model also reveal that high clouds will produce warming everywhere in the atmosphere whereas middle and low clouds will generate cooling as noted by several previous investigators. Moreover, extension of the model to a two-dimensional case is accomplished by incorporating empirical data for the horizontal heat transport. Simulated temperature profiles for the tropics (0–30°) and midlatitude (30–60°) compare closely with the climatological data except in the vicinity of the tropopause. For the subarctic case (60–90°), simulated temperatures are colder than the climatological values within about 5 K in the troposphere. Finally, two-dimensional heat budget analyses reveal that there is a slight gain of energy in the tropical region of the Northern Hemisphere.

1. Introduction

Investigation of the equilibrium temperature of the earth and the atmosphere based on the balance of solar and thermal infrared radiation has been an important subject since the construction of various radiation charts by Elsasser, Möller and Yamamoto in the 1940's and 50's. In a pioneering paper by Manabe and Möller (1961), who cited most of the earlier significant research in this area, comprehensive radiative equilibrium temperatures in clear atmospheres for various latitudes and seasons were obtained utilizing a time marching procedure. Later, Manabe and his associates (Manabe and Strickler, 1964; Manabe and Wetherald, 1967) included the effects of the vertical transport so that realistic temperature profiles may be derived. The method employed was a numerical scheme based on the conservation of potential temperatures which is now known as the convective adjustment.

Since then, the so-called one-dimensional radiative-convective model has been used extensively for the perturbation studies of the external and internal forces and feedback mechanisms on the earth climate using temperature as the fundamental parameter. In a recent review paper, Ramanathan and Coakley (1978) summarized and discussed the merit of the radiative-convective model pertaining to the study of the climate and climatic change of the earth–atmosphere system and cited significant work accomplished prior to 1978. More recently, advanced research work using the radiative-convective model have been carried out by Charlock and Sellers (1980), Wang *et al.* (1981), Hummel and Kuhn (1981), Stephens and Webster (1981), Ramanathan (1981) and Liou and Gebhart (1982) to investigate the influence of various internal factors including carbon dioxide, aerosols and clouds on the temperature field of the earth and the atmosphere.

In this paper, we wish to propose a thermodynamic model which leads to the fundamental equation governing the balance of radiative and turbulent transfer based on which one- and two-dimensional equilibrium temperature fields may be determined. We show that the temperature field in the context of a one-dimensional model is governed by a first-order differential-integro equation involving the lapse rate and the temperature to the fourth power under integration over the altitude covering the entire atmosphere. While the present one-dimensional thermodynamic model represents a more analytic approach to the equilibrium temperature problem, the concept of introducing the vertical eddy transport is similar to, but not exactly the same as, the radiative-convective model described previously. Moreover, we extend the one-dimensional model to a semi-two-dimensional model by incorporating the horizontal heat transport empirically. In Section 3, we present infrared and

solar radiation parameterizations used in this study. In Section 4, we describe a numerical perturbation method developed for radiative-turbulent balance in the one-dimensional case and the methods used in determining the vertical eddy thermal diffusivity in various regions of the atmosphere. Simulation results, physical discussions, and extension of the thermodynamic model to the two-dimensional case are presented in Section 5. Finally, conclusions are given in Section 6.

2. The thermodynamic model

We consider an infinitesimal volume of air in the atmosphere and let the internal energy, the potential energy and the work done within the system be denoted as U, Φ and W, respectively. In the presence of latent heat release, the conservation of the flows of energies in a three-dimensional space requires that

$$\frac{\partial}{\partial t}\rho(U+\Phi+W+Lq_r) + \nabla\cdot\mathbf{v}_r\rho(U+\Phi+W+Lq_r) = -\nabla\cdot\mathbf{F}_r, \quad (2.1)$$

where L denotes the latent heat of vaporization, condensation or sublimation, q_r the saturation mixing ratio, ρ the density of air, $\mathbf{v}_r$ (u, v, w) the velocity vector and $\mathbf{F}_r$ the three-dimensional radiative heat flux (in units of energy per area per time). Since the potential energy of a parcel of air is associated with gravity in the vertical direction, we let $\Phi = \Phi_{z,r}$. Also, $U = C_v T_r$ and $W = PV = R'T_r$, where C_v is the specific heat at constant volume, T_r the temperature, P the pressure, V the volume and R' the universal gas constant for air.

Let

$$T_r = T + T', \quad \mathbf{v}_r = \mathbf{v} + \mathbf{v}', \quad \Phi_{z,r} = \Phi_z + \Phi'_z,$$
$$q_r = q + q' \quad \text{and} \quad \mathbf{F}_r = \mathbf{F} + \mathbf{F}',$$

where parameters with primes denote the deviation from the time average quantity. In the discussion hereafter, T, $\mathbf{v}$, Φ_z, q and $\mathbf{F}$ represent the time-average values. Substituting these definitions into Eq. (2.1) and applying the time average procedure yields

$$\frac{\partial}{\partial t}\rho C_p T + \nabla\cdot\rho(C_p\mathbf{v}T + \mathbf{v}\Phi_z + Lvq) + \nabla\cdot(\overline{\rho C_p\mathbf{v}'T'} + \overline{\rho\mathbf{v}'\Phi'_z} + \overline{\rho Lv'q'}) = -\nabla\cdot\mathbf{F}, \quad (2.2)$$

where C_p is the specific heat at constant pressure and ρ, Φ_z and q are assumed to be independent of time in this model. The second term represents the transport of sensible heat, potential energy and latent heat by the mean motion, while the third term denotes the eddy transport of these quantities in three-dimensional space.

We consider a one-dimensional case in which we neglect the mean vertical velocity as follows:

$$\frac{\partial}{\partial t}\rho C_p T + \frac{\partial}{\partial z}(\overline{\rho C_p w'T'} + \overline{\rho w'\Phi'_z} + \overline{\rho Lw'q'}) = -\frac{\partial F}{\partial z}, \quad (2.3)$$

where w' denotes the vertical velocity deviation. At this point we apply the first-order closure to the turbulent flux, the so-called K-Theory (Taylor, 1915), to obtain

$$\overline{\rho C_p w'T'} + \overline{\rho w'\Phi'_z} + \overline{\rho Lw'q'} = -k_z\rho C_p\left(\frac{\partial T}{\partial z} + \frac{1}{C_p}\frac{\partial\Phi_z}{\partial z} + \frac{L}{C_p}\frac{\partial q}{\partial z}\right) = -k_z\rho C_p\left(\frac{\partial T}{\partial z} + \gamma\right), \quad (2.4)$$

where the moist adiabatic lapse rate is defined by

$$\gamma = \gamma_d + \frac{L}{C_p}\frac{\partial q}{\partial z}, \quad (2.5)$$

with $\gamma_d = g/C_p$, the dry adiabatic lapse rate, and k_z represents the eddy thermal diffusion coefficient. Thus, Eq. (2.2) becomes

$$\frac{\partial}{\partial t}\rho C_p T - \frac{\partial}{\partial z}\left[k_z\rho C_p\left(\frac{\partial T}{\partial z} + \gamma\right)\right] = \frac{\partial}{\partial z}(F_s - F_{IR}). \quad (2.6)$$

Under the equilibrium (i.e., steady-state) condition, a temperature profile will be defined by the balance between the divergence of the solar flux F_s, the infrared flux F_{IR}, and the turbulent flux in terms of the eddy thermal diffusion coefficient. Moreover, since $k_z \to 0$ when $z \to \infty$, and since $F_s(z) = F_{IR}(z)$ at the top of the atmosphere (i.e., $z \to \infty$), by integrating Eq. (2.6) over the atmospheric column from z to ∞ we obtain

$$-k_z\rho C_p\left(\frac{\partial T}{\partial z} + \gamma\right) + F_{IR}(z) = F_s(z). \quad (2.7)$$

Eq. (2.7) relates the incoming solar flux, the outgoing thermal infrared flux, which is basically produced by the atmospheric temperature field, and the turbulent flux in terms of eddy thermal diffusion processes. If the atmospheric lapse rate $(-\partial T/\partial z)$ is greater than the moist adiabatic lapse rate, there will be a positive vertical transport due to the unstable condition caused by the excess of the solar flux. On the other hand, a negative transport occurs when the atmospheric lapse rate is less than the moist adiabatic lapse rate. When the atmospheric lapse rate is equal to the moist adiabatic lapse rate, the temperature field is defined by the balance between the solar and thermal infrared fluxes. Strictly speaking, the moist adiabatic lapse rate depends on the humidity profile as evidenced from Eq. (2.5). It varies from about 4°C km^{-1}

near the ground in warm moist air masses to about 7°C km^{-1} in the middle troposphere. In the temperature numerical experiment, however, we will assign a constant value of 6.5°K km^{-1} for the moist adiabatic lapse rate in calculating the radiative-turbulent equilibrium temperatures. In the following sections, we present orderly parameterizations of the infrared and solar radiation transfer and the turbulent transfer in terms of the eddy thermal diffusion coefficient covering the free atmosphere and the constant flux layer.

3. Parameterization of broadband infrared and solar radiation transfer

Following the analysis given in Liou (1980) for infrared radiative transfer, the net IR flux at a given height z in clear conditions may be written in the form

$$F_{IR}(z) = \int_0^\infty \sigma T^4(z') K(|z - z'|) dz', \qquad (3.1)$$

where T denotes the temperature, σ is the Stefan Boltzmann's constant, and the kernal function is defined by

$$K(|z - z'|) = \begin{cases} -\partial \epsilon^f[|z - z'|, T(z')]/\partial z', & z' \neq 0 \\ [1 - \epsilon^f(z, T_s)]\delta(z - z'), & z' = 0. \end{cases} \qquad (3.2)$$

In Eq. (3.2), δ denotes a delta function and

$$\frac{\partial \epsilon^f[|z - z'|, T(z')]}{\partial z'} = \sum_{i=1}^{6} \frac{\partial \epsilon_i^f\{|\tilde{u}_i(z) - \tilde{u}_i(z')|, T[u_i(z')]}{\partial u_i(z')} \rho_i(z'), \qquad (3.3)$$

where ϵ_i^f (i = 1–5) denote the broadband emissivities for the H_2O rotational band, H_2O vibrational-rotational band, H_2O continuum, and the CO_2 and O_3 bands, respectively, and $\epsilon_6^f = \epsilon_1^f \epsilon_4^f$ is the emissivity for the H_2O–CO_2 overlap correction. In addition, we define $u_1 = u_2 = u_3 = u_w$, $u_4 = u_c$ and $u_5 = u_o$ with u_w, u_c and u_o representing, respectively, the path length for water vapor, carbon dioxide and ozone, and ρ_i denote the corresponding density. In Eq. (3.3), we have incorporated the effects of pressure and temperature on absorption in the path length denoted by $\tilde{u}$ for the calculation of broadband emissivities in accordance with the parameterization scheme developed by Liou and Ou (1981). On the basis of Eq. (3.1), we may interpret that the net IR flux at any given atmospheric height is the sum of the Planck fluxes emitted from the entire atmosphere and the surface to this height weighted by a proper kernel function which is in reference to this particular height. In addition, we see that the kernel function in reference to an atmospheric layer is given by the slope of the emissivity curve.

To economize the computational effort, we carry out numerical fits to the individual emissivity curve in terms of polynomial functions in the forms

$$\ln \epsilon_i^f(u_i) = \sum_{l=0}^{3} a_{l,i} \bar{u}_i^l, \quad \bar{u}_i = (2 \log_{10} u_i - \bar{a})/\bar{b}, \qquad (3.4)$$

where $\bar{a} = \log_{10}(u_{i,\max}\ u_{i,\min})$, $\bar{b} = \log_{10}(u_{i,\max}/u_{i,\min})$, and $u_{i,\max}$ and $u_{i,\min}$ denote the maximum and minimum path lengths used in the numerical fitting. For water vapor (i = 1, 2, 3, 6), carbon dioxide (i = 4) and ozone (i = 5), they are from 10^{-7} to 10 g cm^{-2}, 10^{-7} to 0.2 g cm^{-2}, and 10^{-7} to 10^{-3} g cm^{-2}, respectively. Eq. (3.4) fits all individual emissivity curves derived in the work of Liou and Ou (1981) within 2%. Table 1 lists values for the empirical coefficients $a_{l,i}$ for four temperatures covering the likely range of the atmospheric temperature. For the CO_2–H_2O overlap band, four CO_2 path lengths are utilized in the fitting. For other intermediate temperatures and CO_2 path lengths, interpolations between these values may be carried out to obtain the desirable emissivity. For cloudy atmospheres, parameterization schemes developed by Liou and Ou (1981) are used in the numerical calculation.

For the parameterization of broadband solar radiation transfer, we consider first that absorption of solar fluxes in a clear atmosphere is mainly confined within the UV (due to ozone) and near infrared (due to water vapor and carbon dioxide) spectral regions. If we let the cosine of the solar zenith angle θ_0 be μ_0, then the total direct downward solar flux in nonscattering atmospheres covering the entire solar spectrum normal to the layer of stratification is given by

$$F^{\downarrow}(z) = \mu_0 S[1 - A(z)], \qquad (3.5)$$

where the broadband absorptivity due to the absorption of O_3, H_2O and CO_2 may be written in the form

$$A(z) = \frac{1}{S}\int_0^\infty F_\lambda(0) A_\lambda(u/\mu_0) d\lambda = A(u_0/\mu_0) + A(u_w/\mu_0) + \epsilon A_5(u_c/\mu_0) \approx \sum_i A_i(u_0/\mu_0) f_i + \sum_i A_i(u_w/\mu_0) f_i + \epsilon A_5(u_c/\mu_0), \qquad (3.6)$$

and the solar constant is defined by

$$S = \int_0^\infty F_\lambda(0) d\lambda.$$

Note that we have set $f_i \approx F_\lambda(0) d\lambda$ and ϵ is the CO_2–H_2O overlap correction at the 2.7 μm band described below.

For water vapor and carbon dioxide absorption, we make use of the empirical formulas derived from laboratory measurements as presented by Liou and Sasamori (1975). Solar water vapor absorption bands include 0.94, 1.1, 1.37, 1.87, 2.7 and 3.2 μm bands. We used the subscript i (1–6) to denote these bands.

TABLE 1. Coefficients of broadband emissivity values for the six infrared bands.

	i	$a_{0,i}$	$a_{1,i}$	$a_{2,i}$	$a_{3,i}$
T = 203 K	1	−0.16378+001	0.31523+001	−0.28231+001	0.10998+001
	2	−0.98069+001	0.91563+001	−0.54110+000	−0.27859+000
	3	−0.58349+001	0.54245+001	−0.34050+001	0.85649−002
	4	−0.36277+001	0.38374+001	−0.28966+001	−0.99049+000
	5	−0.67785+001	0.42930+001	−0.95681+000	−0.55536+000
	6 u_c = 0.35900−005	−0.11659+002	0.76658+001	−0.23614+001	−0.67473+000
	0.12900−003	−0.11628+002	0.76834+001	−0.23500+001	−0.67884+000
	0.46400−002	−0.11658+002	0.76970+001	−0.23417+001	−0.68208+000
	0.16700+000	−0.11723+002	0.77077+001	−0.23358+001	−0.68466+000
T = 233 K	1	−0.18865+001	0.32475+001	−0.27705+001	0.10903+001
	2	−0.95159+001	0.91534+001	−0.52756+000	−0.26671+000
	3	−0.50133+001	0.53627+001	−0.34506+001	0.10991−001
	4	−0.35627+001	0.38374+001	−0.28966+001	−0.99049+000
	5	−0.63805+001	0.42918+001	−0.95672+000	−0.55860+000
	6 u_c = 0.35900−005	−0.80514+001	0.76658+001	−0.23241+001	−0.67473+000
	0.12900−003	−0.80210+001	0.76834+001	−0.23127+001	−0.67884+000
	0.46400−002	−0.80508+001	0.76970+001	−0.23045+001	−0.68208+000
	0.16700+000	−0.81159+001	0.77077+001	−0.22985+001	−0.68466+000
T = 263 K	1	−0.21226+001	0.33251+001	−0.27277+001	0.10832+001
	2	−0.93430+001	0.91512+001	−0.51723+000	−0.25749+000
	3	−0.44264+001	0.53278+001	−0.34806+001	0.79503−002
	4	−0.35648+001	0.38374+001	−0.28966+001	−0.99049+000
	5	−0.61317+001	0.42910+001	−0.95628+000	−0.56004+000
	6 u_c = 0.35900−005	−0.67591+001	0.76658+001	−0.23108+001	−0.67473+000
	0.12900−003	−0.67287+001	0.76834+001	−0.22994+001	−0.67884+000
	0.46400−002	−0.67585+001	0.76970+001	−0.22912+001	−0.68208+000
	0.16700+000	−0.68236+001	0.77077+001	−0.22852+001	−0.68466+000
T = 293 K	1	−0.23454+001	0.33888+001	−0.26927+001	0.10777+001
	2	−0.92462+001	0.91495+001	−0.50918+000	−0.25017+000
	3	−0.39991+001	0.53068+001	−0.35005+001	0.42209−002
	4	−0.36093+001	0.38374+001	−0.28966+001	−0.99049+000
	5	−0.59797+001	0.42904+001	−0.95611+000	−0.56109+000
	6 u_c = 0.35900−005	−0.67240+001	0.76658+001	−0.23104+001	−0.67473+000
	0.12900−003	−0.66936+001	0.76834+001	−0.22990+001	−0.67884+000
	0.46400−002	−0.67235+001	0.76970+001	−0.22908+001	−0.68208+000
	0.16700+000	−0.67885+001	0.77077+001	−0.22848+001	−0.68466+000

Carbon dioxide absorption is only significant in the 2.7 μm band which overlaps with water vapor absorption. In accordance with laboratory measurements by Howard *et al.* (1956), total absorption within the 2.7 μm band (i = 5) is given by $A_5(u_w, u_c) = A_5(u_w) + \epsilon A_5(u_c)$, where the overlap correction based on the experimental fitting has the form $\epsilon[A_5(u_w)] = a + bA_5(u_w)$, where $a = 0.75$ and $b = 0.48$ for $A_5(u_w) \geqslant 300$ cm^{-1}, and $a = 1$ and $b = 1.12$ for $A_5(u_2) < 300$ cm^{-1}. For ozone absorption the band absorptivity is simply defined by $A_i(u_0/\mu_0) = 1 - \exp(-k_i u_0/\mu_0)$, where the absorption coefficients k_i are taken from the data obtained by Inn and Tanaka (1953) and Vigroux (1953) as presented in the *Handbook of Geophysics* (1961).

To include the scattering and surface reflection effects in the calculations of the solar net flux and heating rate we consider an atmosphere containing a defined scattering layer whose flux reflection $r(\mu_0)$ and transmission $t(\mu_0)$ properties are known. We also consider a Lambertian surface with an albedo of r_s. Taking into account multiple reflections between the surface and scattering layer and separating the direct (associated with μ_0) and diffuse solar fluxes, the net solar fluxes above and below a defined scattering layer may be described, respectively, by the following equations:

$$F_s(z) = F^{\downarrow}(z) - F^{\downarrow}(z_t)\{r + G[1 - \bar{A}(z_b)]\bar{t}\} \times [1 - \bar{A}(z - z_t)], \quad z > z_t, \quad (3.7)$$

$$F_s(z) = F^{\downarrow}(z_t)\{t + G[1 - \bar{A}(z_b)]\bar{r}\}[1 - \bar{A}(z_b - z)] - F^{\downarrow}(z_t)G[1 - \bar{A}(z)], \quad z < z_b, \quad (3.8)$$

where we define a non-dimensional upward diffuse component called the generation function at the surface involving multiple reflections between the scattering layer and surface in the form

$$G = t[1 - A(z_b)]r_s\{1 - [1 - \bar{A}(z_b)]^2\bar{r}r_s\}^{-1}. \quad (3.9)$$

In these equations, $\bar{r}$ and $\bar{t}$ denote the global (diffuse)

reflection and transmission for the scattering layer defined in Liou and Wittman (1979) and the diffuse absorptivity due to gaseous absorption $\bar{A} = A[1.66\, u(z)]$. In Eq. (3.7), the first component of the second term on the right-hand side denotes reflection of the direct solar flux reaching the top of the scattering layer through $r(\mu_0)$. The second component represents the upward diffuse contribution originated by the generation function G which is the sum of the reflection of direct and diffuse components at the surface. In Eq. (3.8), on the other hand, the first term represents the downward flux resulting from the direct and diffuse transmission, while the second term is the upward flux due to the diffuse reflection.

In cloudy conditions, values of r, t, $\bar{r}$ and $\bar{t}$ as functions of the solar zenith angle and liquid water content for different cloud types are computed from the parameterization equations presented by Liou and Wittman (1979). However, in clear conditions, z_t is set to be 10 km and $z_b = 0$. The value of reflection due to Rayleigh scattering is taken from the parameterized equation derived by Lacis and Hansen (1974), i.e., $r = r_a = 0.28(1 + 6.43\mu_0)^{-1}$. For net fluxes above z_t, we use Eqs. (3.7) and (3.9), except the flux transmission t is replaced by $1 - r_a - A(z_t)$, where $A(z_t)$ is the absorptivity due primarily to water vapor. Note that $\bar{A}(z_b) = 0$. For the net flux below z_t which is in the water vapor absorption layer mixed with Rayleigh scattering, the following parameterization equation is employed:

$$F_s(z) = F^{\downarrow}(z_t)[1 - r_a - \bar{A}(z_t - z)] - F^{\downarrow}(z_t)tr_s[1 - \bar{A}(z)] + F^c, \quad (3.10)$$

where the first and second terms represent the upward and downward fluxes, respectively, and we add a correction term F^c so that when $z = z_t$, the net flux is the same as that given in Eq. (3.7). In this manner, effects of Rayleigh scattering on the transfer of solar fluxes are approximately taken into consideration both in ozone and water vapor layers. Note that the computation of the correction term F^c is done numerically in the parameterization program using Eqs. (3.7) and (3.10) when $z = z_t$.

In Fig. 1 are shown the comparisons of the solar net fluxes and heating rates computed from the parameterization scheme and a more exact and comprehensive radiative transfer program developed at the University of Utah over the last few years (Freeman and Liou, 1979; Liou and Wittman, 1979). A fraction of daytime of 0.5 along with values depicted in the diagram are used in the computation. Agreement between these two methods is within ~0.02°C day^{-1} (solar day is used here) and 5 W m^{-2} for solar heating rates and net fluxes, respectively. Below about 10 km, solar heating is basically produced by absorption of H_2O. Between about 10–15 km, absorption of CO_2 contributes to within about 0.1°C day^{-1}

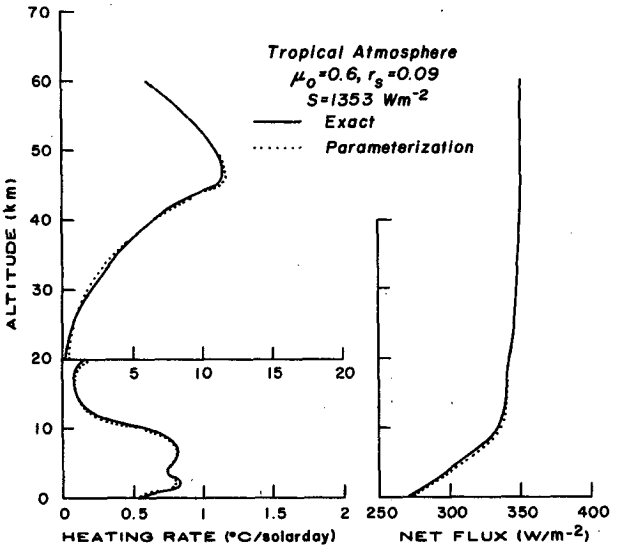

FIG. 1. Comparisons of solar heating rates and net fluxes computed from the flux parameterization scheme with results from a more exact radiative transfer program.

heating rates. Above 15 km, large solar heating is exclusively caused by O_3 absorption. The net solar flux ranges from about 350 W m^{-2} at the top of the atmosphere to about 270 W m^{-2} at the surface. A series of comparisons between the parameterization and more exact programs involving different atmospheric conditions and solar zenith angles have also been performed. We found that the present parameterization program for net flux and heating rate computations, which has not been presented in our previous publications, has an accuracy similar to the case depicted here.

4. Numerical procedures for the computations of equilibrium temperatures

a. Radiative-turbulent equilibrium

In reference to Eqs. (2.7) and (3.1), the basic equation governing a radiative-turbulent atmosphere may be written in the form

$$-k_z\rho C_p\left(\frac{\partial T}{\partial z} + \gamma\right) + \int_0^\infty \sigma T^4(z')K(|z - z'|)dz' = F_s(z). \quad (4.1)$$

This is a first-order differential-integro thermodynamic equation. In order to derive a solution for the temperature field, we first determine the radiative equilibrium temperature T_0 which is defined by the balance between solar and infrared fluxes as

$$\int_0^\infty \sigma T_0^4(z')K(|z - z'|)dz' = F_s(z). \quad (4.2)$$

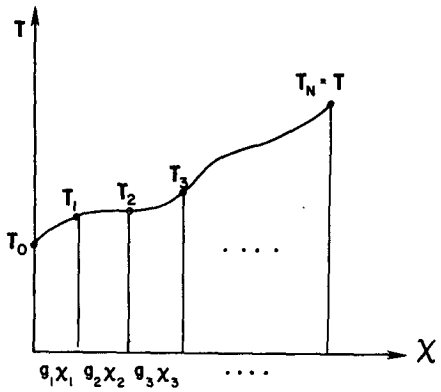

$$\chi(z) = [\sigma T^4(z) - \sigma T_0^4(z)]/\gamma c \rho C_p$$

FIG. 2. Configuration of the temperature perturbation with respect to a perturbation parameter χ defined in the figure where T_0 is the radiative equilibrium temperature and T the equilibrium temperature to be obtained.

We wish to derive a perturbation equation from which the thermal equilibrium temperature can be computed numerically in reference to a perturbation parameter χ defined by the difference between the Planck functions of radiative-turbulent and pure radiative temperatures; χ and a number of other parameters are defined by

$$\left.\begin{aligned} \chi(z) &= [\sigma T^4(z) - \sigma T_0^4(z)]/k', \quad k' = \gamma c \rho C_p \\ H(|z - z'|) &= K(|z - z'|)/f(z), \quad f(z) = k_z/c \end{aligned}\right\}, \tag{4.3}$$

where c is a scaling constant such that $f(z) = 1$ when $z = 0$, and k' also is a constant. Thus, by virtue of Eqs. (4.2) and (4.3), Eq. (4.1) may be rewritten in the form

$$1 + \frac{1}{\gamma}\frac{dT}{dz} = \int_0^\infty \chi(z')H(|z - z'|)dz'. \tag{4.4}$$

We now let the perturbation parameter be expressed by (Carrier, 1974)

$$\chi = \sum_{n=1}^{N} g_n \chi_n, \tag{4.5}$$

where g_n are arbitrary constants. In reference to Fig. 2 we wish to find an equilibrium temperature T from the radiative equilibrium temperature T_0 with respect to the components of the perturbation parameter χ_n. Using the Taylor series expansion, each adjacent temperature may be expressed by

$$\begin{aligned} T_m &= T_{m-1} + \sum_{n=1}^{N} \frac{1}{n!}\left(\frac{\partial^n T}{\partial \chi^n}\right)_{T=T_{m-1}} (g_m\chi_m)^n \\ &= T_{m-1} + \left(\frac{\partial T}{\partial \chi}\right)_{T=T_{m-1}} (g_m\chi_m) + g_m{}^2 R_m, \\ &\qquad m = 1, 2, \ldots, N, \end{aligned} \tag{4.6}$$

where the Taylor series expansion terms higher than the first order are defined by

$$g_m{}^2 R_m = T_m - T_{m-1} - \left(\frac{\partial T}{\partial \chi}\right)_{T=T_{m-1}} (g_m\chi_m). \tag{4.7}$$

Also, from the definition of χ in Eqs. (4.3) and (4.5), the perturbation temperature can be expressed by

$$\sigma T_m{}^4 = \sigma T_0{}^4 + k' \sum_{n=1}^{m} g_n\chi_n. \tag{4.8}$$

From Eq. (4.6), summing all the perturbation temperatures leads to

$$\begin{aligned} T &= T_N \\ &= T_0 + \sum_{m=1}^{N} \left[\left(\frac{\partial T}{\partial \chi}\right)_{T=T_{m-1}} (g_m\chi_m) + g_m{}^2 R_m\right]. \end{aligned} \tag{4.9}$$

On substituting Eq. (4.9) into Eq. (4.4), we find

$$\begin{aligned} 1 + \frac{1}{\gamma}\left\{\frac{dT_0}{dz} + \sum_{m=1}^{N} \frac{d}{dz}\right. &\times \left.\left[\left(\frac{\partial T}{\partial \chi}\right)_{T=T_{m-1}} (g_m\chi_m) + g_m{}^2 \frac{dR_m}{dz}\right]\right\} \\ &= \sum_{n=1}^{N} g_n \int_0^\infty \chi_n(z')H(|z - z'|)dz'. \end{aligned} \tag{4.10}$$

From Eq. (4.8), the derivative of the perturbation temperature with respect to χ defined in Eq. (4.5) is

$$\left(\frac{\partial T}{\partial \chi}\right)_{m-1} = k'(4\sigma T_{m-1}^3)^{-1}. \tag{4.11}$$

Moreover, we set $g_{m+1} = g_m{}^2$ and arbitrarily select $g_1 = 1$. Upon collecting terms with the same order in g_1 and using Eqs. (4.7) and (4.11) we obtain the perturbation equations:

$$\begin{aligned} 1 + \frac{1}{\gamma}\left[\frac{dT_0}{dz} + \frac{d}{dz}\left(\frac{k'}{4\sigma T_0{}^3}\chi_1\right)\right] &= \int_0^\infty \chi_1(z')H(|z - z'|)dz', \end{aligned} \tag{4.12}$$

$$\begin{aligned} \frac{d}{dz}\left(T_{m-1} - T_{m-2} - \frac{k'}{4\sigma T_{m-2}^3}\chi_{m-1}\right) + \frac{d}{dz}\left(\frac{k'}{4\sigma T_m{}^3}\chi_m\right) &= \gamma \int_0^\infty \chi_m(z')H(|z - z'|)dz', \\ m = 2, 3, \ldots, N. \end{aligned} \tag{4.13}$$

Since $T_0(z)$ has been determined previously from Eq. (4.2), Eqs. (4.12) and (4.13), representing the same type of equations, can be successively used to obtain χ_1 and T_1 and χ_m and T_m (i.e., $\sigma T_m{}^4 = \sigma T_{m-1}^4 + k'\chi_m$) by a similar numerical procedure. Utilizing finite difference formats for these equations, the unknown

variable χ_m as a function of z can also be evaluated from a standard matrix inversion method. The convergence using the present perturbation scheme is extremely efficient. Normally, three to four computations are sufficient to converge the temperature solution within about 0.1%.

b. *Determination of eddy thermal diffusion coefficient*

In this study, the eddy thermal diffusion coefficient is calculated and/or taken from previous published analyses. We do so by dividing the atmosphere into a number of regions.

In the constant flux layer ($z \leqslant 100$ m), the eddy thermal diffusion coefficient may be written

$$k_z = \frac{\alpha}{\phi_m} u_* kz, \tag{4.14}$$

where u_* denotes the friction velocity and k is known as von Karman's constant. In accordance with the measured data presented by Businger *et al.* (1971), the ratio of the eddy transfer coefficient and a dimensionless wind shear are, respectively, given by

$$\alpha = k_z/k_m = \begin{cases} 1.35(1 - 9\zeta)^{1/2}(1 - 15\zeta)^{-1/4}, & \text{unstable} \\ (1 + 4.7\zeta)(0.74 + 4.7\zeta)^{-1}, & \text{stable,} \end{cases} \tag{4.15}$$

$$\phi_m = \frac{kz}{u_*}\frac{\partial \bar{u}}{\partial z} = \begin{cases} (1 - 15\zeta)^{-1/4}, & \text{unstable} \\ (1 + 4.7\zeta), & \text{stable.} \end{cases} \tag{4.16}$$

In these equations, k_m is the eddy viscosity, $\partial\bar{u}/\partial z$ is the mean wind shear, and the dimensionless height is defined by

$$\zeta \propto \left(\frac{kz}{u_*}\right)^2 \frac{g}{T}\left(\frac{\partial T}{\partial z} + \gamma_d\right), \tag{4.17}$$

where g is the gravitational acceleration and γ_d the adiabatic lapse rate. In the calculations, we take $k = 0.4$ and $u_* = 40$ cm s^{-1}. Under the unstable condition, we note that $|-9\zeta| \geqslant 1$. Upon inserting Eqs. (4.15)–(4.17) into Eq. (4.14) we find k_z has a similar expression as the one derived by Priestley (1959) based on the similarity method. Priestley's similarity model has been adapted by Gierasch and Goody (1968) in the study of the temperature structure of the Martian atmosphere.

In the troposphere between 100 m and the tropopause (~100 mb), we utilize the mixing length theory to calculate k_z, i.e.,

$$k_z \propto \overline{l^2}\left|\frac{\partial \bar{u}}{\partial z}\right|, \tag{4.18}$$

where the mixing length l is set to be 30 m and the mean wind shear is approximated by a linear equation in height in the form

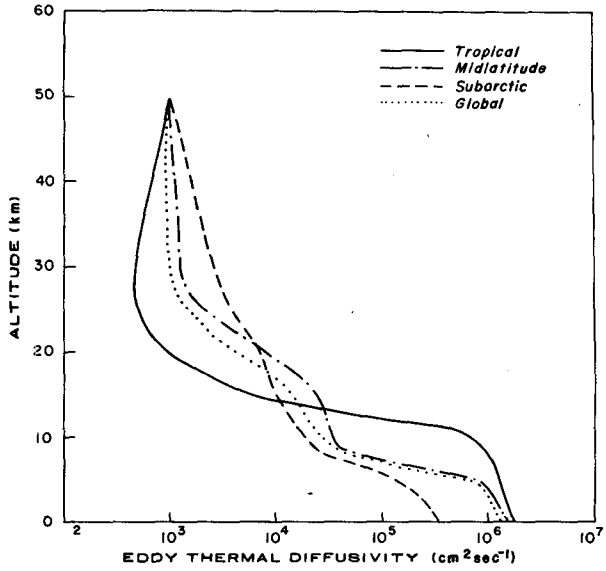

FIG. 3. Eddy thermal diffusion coefficient for tropical, midlatitude, subarctic and global (standard) atmospheres.

$$\frac{\partial \bar{u}}{\partial z} = az + b, \tag{4.19}$$

where a and b are estimated from the known k_z values at the top of the constant flux layer and the tropopause. The latter k_z values for various atmospheric profiles are computed from those presented by Reed and German (1965). In their study, the eddy thermal diffusion coefficients for the Northern Hemisphere are listed according to seasons and for layers at 100, 50 and 30 mb. Finally, a value of 10^{-3} g cm^{-1} s^{-1} is employed for ρk_z at a height of 50 km (Hunt, 1981).

Fig. 3 shows the eddy thermal diffusion coefficient for tropical, midlatitude, subarctic and global (standard) atmospheric profiles based on the aforementioned computational procedures. The computation of these coefficients makes use of the radiative equilibrium temperature profile under clear conditions. Physically, we may imagine that in the context of a steady-state radiative equilibrium, a temperature profile is established but it is generally unstable since too much solar energy is stored at the surface. To achieve a thermal equilibrium, the vertical eddy transport must subsequently take place in which the eddy thermal diffusion process is responsible for the stability of the temperature field in the earth–atmosphere system. The eddy thermal diffusivity k_z has the largest values in the troposphere under the tropical condition. Near the surface, except the subarctic condition, k_z has values on the order of 10^6 cm^2 s^{-1}. In the stratosphere, k_z values are two to three orders of magnitude less than those in the troposphere. Since the subarctic region is generally stable, k_z values in the troposphere are relatively small.

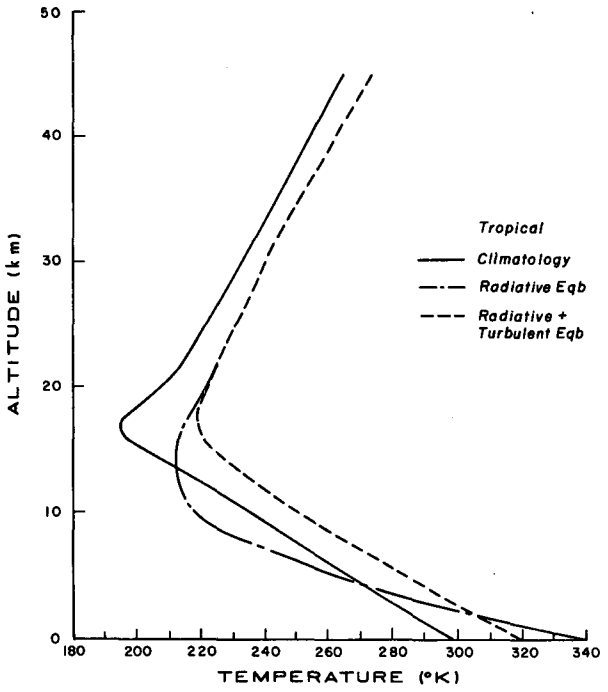

FIG. 4. Radiative equilibrium and radiative-turbulent equilibrium temperatures in a clear tropical atmosphere in reference to climatological data.

5. Simulation results and discussions

a. One-dimensional model

In Fig. 4 are shown one-dimensional temperature profiles corresponding to pure radiative and radiative-turbulent equilibriums. The objective of presenting this figure is to illustrate the efficiency of the present perturbation method in the determination of a temperature profile. For this purpose we have used tropical atmospheric water vapor and ozone profiles with no cloud. Obviously, other profiles may be used for this demonstration. As is well understood, the radiative equilibrium temperature is too warm near the surface and too cold in the tropopause (Manabe and Strickler, 1964). Vertical thermal eddy transport brings the temperature structure into a stable mode. Generally, to achieve a radiative-turbulent equilibrium, three to four perturbation iterations are sufficient. The solid curve in the figure is the climatological temperature profile for reference purposes. Since clouds are not considered in the exercises, we will make no comparison between the present result and climatological data.

In order to simulate temperature profiles for various latitudinal belts and global conditions based on a steady-state model we need to derive averaged annual solar zenith angles and surface albedo values in solar flux calculations. Cosines of the solar zenith angles μ_0 derived are 0.6, 0.436, 0.296 and 0.5 for tropical, midlatitude, subarctic and global conditions, respectively. Using the zonally dependent surface albedos tabulated by Katayama (1966) for the Northern Hemisphere and Sasamori *et al.* (1972) for the Southern Hemisphere and taking into account the areas involved, the respective surface albedos for tropical, midlatitude, subarctic and global conditions are 0.091, 0.116, 0.519 and 0.158. The length of the solar day in the annual case is 12 h and the solar constant used is 1353 W m^{-2}. In addition, cloud types and their base and top heights and fractional coverages for the zonal belts are derived from the latitudinal data provided by London (1957) for the Northern Hemisphere and Sasamori *et al.* (1972) for the Southern Hemisphere. Results of the cloud data for the tropical, midlatitude, subarctic and global conditions are listed in Table 2.

In Table 3, solar and infrared radiative properties of various cloud types are listed. These radiative properties are derived from the parameterization equations presented by Liou and Wittman (1979). The particle size distributions for a number of cloud types used in the calculations have been described in that paper. Since their paper did not provide parameterization equations for Ns and Cb, we have used the equation for middle clouds in calculating these radiative properties. It should be noted that the mean particle size for the middle cloud is larger than that for the low cloud (basically fair weather cumulus). For this reason, while the thicknesses of these clouds are about the same, middle cloud shows a larger reflection value. Reflection and transmission values for Ns and Cb are about the same because their radiative properties approach asymptotic values which do not significantly depend on the increase of the liquid water content. Except the high cloud and St, low and middle clouds have large reflection values (70–80%) produced by large mean optical depths which are closely related to the cloud liquid water content and solar zenith angle. Owing to the variation of the mean solar zenith angle corresponding to different atmospheric conditions, solar radiative properties of low and middle clouds vary slightly. This variation is rather significant for optically thin clouds. For example, a high cloud reflects only 7.7% in the tropical case, but the reflection value increases to more than a factor of 2 in the subarctic case. Reflection values for a thin stratus range from 0.477 to 0.595 corresponding to tropical and subarctic conditions, respectively.

In the thermal infrared, all clouds are assumed to be black, except high clouds whose mean emissivity, transmissivity and reflectivity also are derived from the parameterization equation given by Liou and Wittman (1979). High cloud is about half-black using the same vertical liquid water content as in the solar case. It is quite evident that the infrared emissivity of high cloud will be more pronounced in the determination of the temperature field than the reflection

TABLE 2. Climatological cloud base (H_b) and top (H_t) heights and fracitonal cloudiness (η) for tropical, midlatitude, subarctic and globally averaged atmospheres. H_b and H_t are in units of km.

Cloud type	Tropical			Midlatitude			Subarctic			Global		
	H_b	H_t	η	H_b	H_t	η	H_b	H_t	η	H_b	H_t	η
Low	1.80	2.75	0.116	1.72	2.47	0.096	1.27	1.83	0.069	1.70	2.52	0.102
Middle	4.10	5.15	0.056	3.17	3.57	0.064	2.18	2.79	0.102	3.50	4.26	0.065
Ci	10.20	11.90	0.136	8.74	10.44	0.135	7.04	8.74	0.153	9.24	10.94	0.138
Ns	1.48	4.21	0.046	1.37	3.18	0.088	0.85	2.20	0.113	1.35	3.56	0.070
Cb	1.80	6.12	0.032	1.72	4.67	0.028	1.27	3.19	0.025	1.70	5.20	0.030
St	1.48	1.58	0.066	1.37	1.47	0.138	0.85	0.95	0.156	1.35	1.45	0.104
Clear	—	—	0.546	—	—	0.450	—	—	0.383	—	—	0.489

(albedo) effect since most of the solar flux transmits through it. On the contrary, however, for middle and low clouds, the cloud albedo will have a predominant influence on the temperature field determination, especially the surface temperature, because a large portion of the solar flux is reflected back to the atmosphere above the cloud.

On utilizing the water vapor and ozone concentration profiles depicted in Fig. 5 and the cloud data listed in Table 2, we carry out numerical computations for the radiative-turbulent equilibrium temperatures of clear and a number of cloudy conditions for a standard global atmosphere. In Fig. 6 we observe that a high cloud produces a warming effect everywhere in the troposphere and low stratosphere. This warming is as large as ~15 K near the surface. As pointed out previously, it is basically caused by the infrared greenhouse effect. For middle and low clouds, we see a significant reduction of the temperature ~30–40 K below about 30 km, in reference to a clear atmosphere. Middle cloud produces more cooling than low cloud because the former has a larger reflectivity resulting from a larger particle size distribution employed in prescribing the solar radiative properties.

In their pioneering paper, Manabe and Wetherald (1967) performed extensive numerical experiments on the influence of high, middle and low clouds on the equilibrium temperature in a radiative-convective model. It appears interesting to compare earlier and present cloud results. For comparison purposes, we have selected high, middle and low cloud cases where 100% cloud covers were used in their paper. It should be noted that their experiments included overlap of three cloud types. For high clouds, the emissivity derived in the present investigation and used in their study (half-black) is about the same but their reflectivity (20%) is higher than ours (10.5%). Also, 7% middle cloud and 31% low cloud are involved in their experiment. For these reasons, the present study produces a higher temperature (318 K) than their value of 284.2 K. In the middle cloud condition, we derived a higher cloud reflectivity of 83% as compared to their value of 48%. Owing to the large difference in solar reflectivity, we show a much colder surface temperature of 226 K as compared to their value of 252 K. Lastly, while the solar reflectivity and position of the low cloud are about the same in both studies, their surface temperature value (229 K) is lower than that of the present study of 250 K. This is due in part to

TABLE 3. Solar and infrared radiative properties of clouds with thicknesses listed in Table 2.

Cloud type	Tropical		Midlatitude		Subarctic		Global	
	r	t	r	t	r	t	r	t
				Solar Radiative Properties				
Low	0.766	0.076	0.766	0.103	0.767	0.130	0.769	0.092
Middle	0.805	0.037	0.794	0.084	0.848	0.037	0.825	0.032
Ci	0.077	0.911	0.125	0.858	0.171	0.804	0.105	0.880
Ns	0.830	0.032	0.840	0.022	0.850	0.016	0.835	0.026
Cb	0.832	0.030	0.843	0.020	0.851	0.015	0.837	0.025
St	0.477	0.416	0.551	0.351	0.595	0.316	0.524	0.375
	ϵ	t	ϵ	t	ϵ	t	ϵ	t
				Infrared Radiative Properties				
Ci	0.475	0.532	0.475	0.532	0.475	0.532	0.475	0.532
Other clouds	1	0	1	0	1	0	1	0

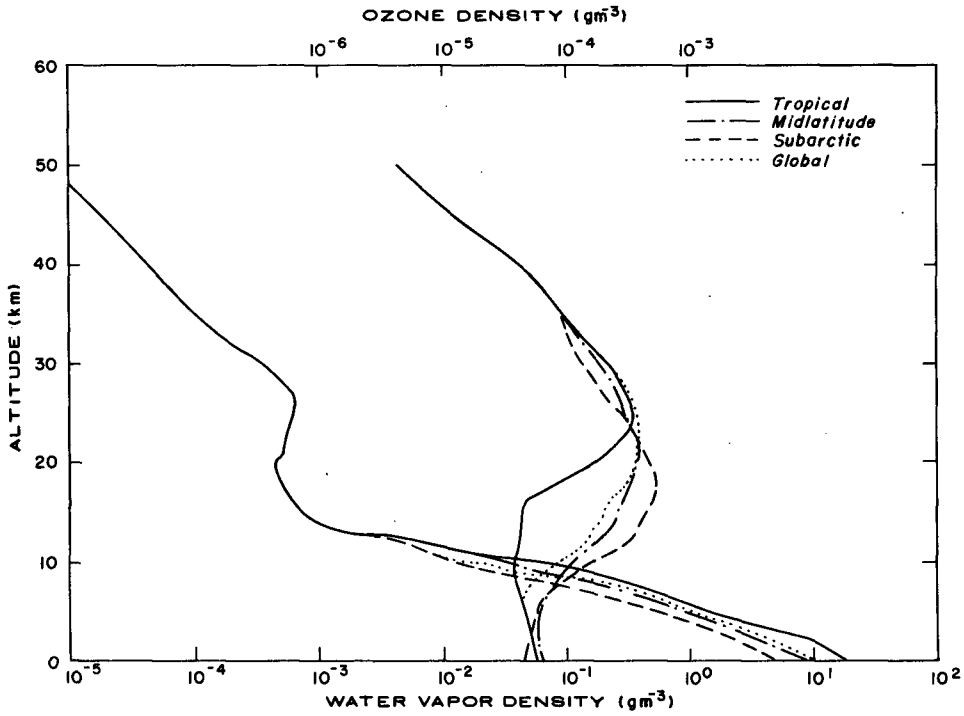

FIG. 5. Climatological water vapor and ozone profiles corresponding to tropical, midlatitude, subarctic and global conditions.

the addition of middle and high cloud layers in their calculations which effectively increases the mean optical depth of the cloud field.

Taking into account the percentage of the cloud cover listed in Table 2 for the global condition, we obtain a steady-state temperature profile which would represent the temperature field resulting from the distribution of water vapor, ozone and clouds. Depicted in Fig. 7 is the temperature profile derived from the present one-dimensional model. Also shown for comparison purposes are the standard atmospheric temperature profile and the temperature profiles derived by Manabe and Wetherald (1967) and by Ramanathan (1976). The former authors utilized a numerical scheme now called the convective adjustment, while the latter author determines the surface temperature and the height of the tropopause and uses a lapse rate of 6.5°C km^{-1}. While the present model represents a more analytic approach to the equilibrium temperature problem, it reproduces the standard tropospheric temperature profile rather closely. In the stratosphere from above about 20 to 40 km, the present model produces colder temperatures than the standard atmospheric temperature profile. There are also slight differences between the present model and other pioneering studies. These differences are clearly attributed to different solar and infrared radiation schemes used in calculating solar and infrared heating rates.

Although it is physically understood that the applications of the one-dimensional radiative-convective model are primarily for numerical simulations of temperature profiles under a global condition, use of different atmospheric water vapor and ozone profiles corresponding to various latitudes for the study of temperature perturbations is not uncommon. In

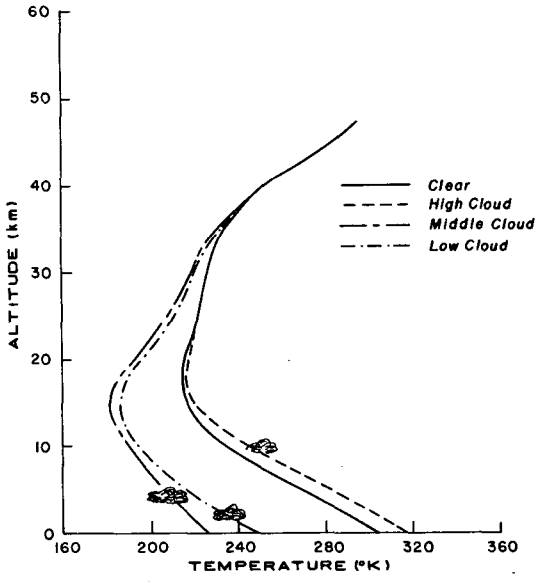

FIG. 6. Effects of high, middle and low clouds on equilibrium temperature in a standard atmospheric condition.

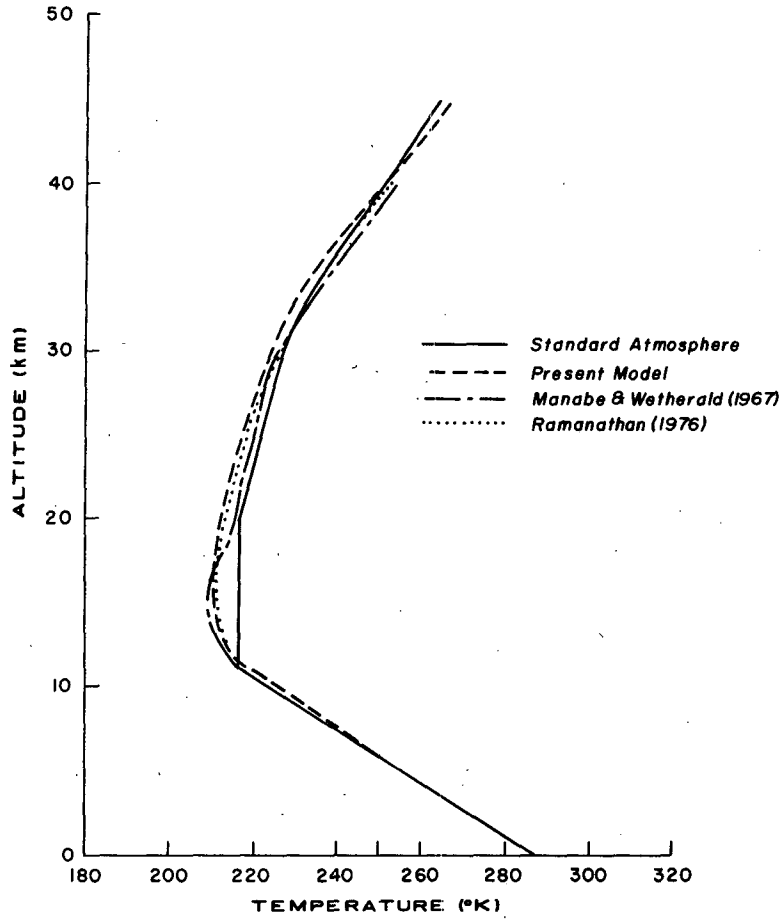

FIG. 7. Comparisons of the equilibrium temperature derived from the present model with the standard atmospheric temperature profiles and other pioneering results.

their pioneering papers on the subject, Manabe and Strickler (1964) and Manabe and Wetherald (1967) performed extensive numerical experiments to investigate equilibrium temperatures for various latitudes in the Northern Hemisphere. Stephens and Webster (1981) also carried out sensitivity experiments on the effects of the surface albedo and cloud position on the equilibrium surface temperature for various latitudes utilizing a one-dimensional radiative-convective model. Sarachik (1978), on the other hand, used a one-dimensional model to study the interaction and coupling of atmosphere and ocean on the temperature field in the tropics. More recently, Lindzen *et al.* (1982) carried out an important sensitivity analysis concerning the convective model employed in the one-dimensional model in the calculation of climate impact of doubling CO_2. Their proposed physical parameterization on cumulus convection is basically applicable to the tropics.

While it is not the intent of the present study to perform sensitivity analyses utilizing parameters corresponding to either standard or other atmospheric conditions, it is intended to investigate quantitatively the derivation of numerically derived temperature profiles from climatological values using the climatological data involving water vapor and ozone profiles, average cloud conditions, mean solar zenith angles and mean surface reflectivities for various latitudinal belts. Based on this investigation using the one-dimensional model, it is our objective to explore the possible extension of the radiative-turbulent equilibrium to a two-dimensional space.

Fig. 8 illustrates three atmospheric temperature profiles derived from the present model (dashed lines) corresponding to tropical, midlatitude and subarctic climatological water vapor, ozone and cloud profiles depicted in Fig. 5 and Table 2. Also depicted in the figure are three climatological temperature profiles (solid lines) for comparison purposes. For the tropical atmosphere (0–30°), the simulation temperatures are higher than climatological values everywhere in the troposphere (~5 K) and stratosphere (~10 K). The maximum difference occurs in the vicinity of the tropopause. High temperatures in the tropical atmo-

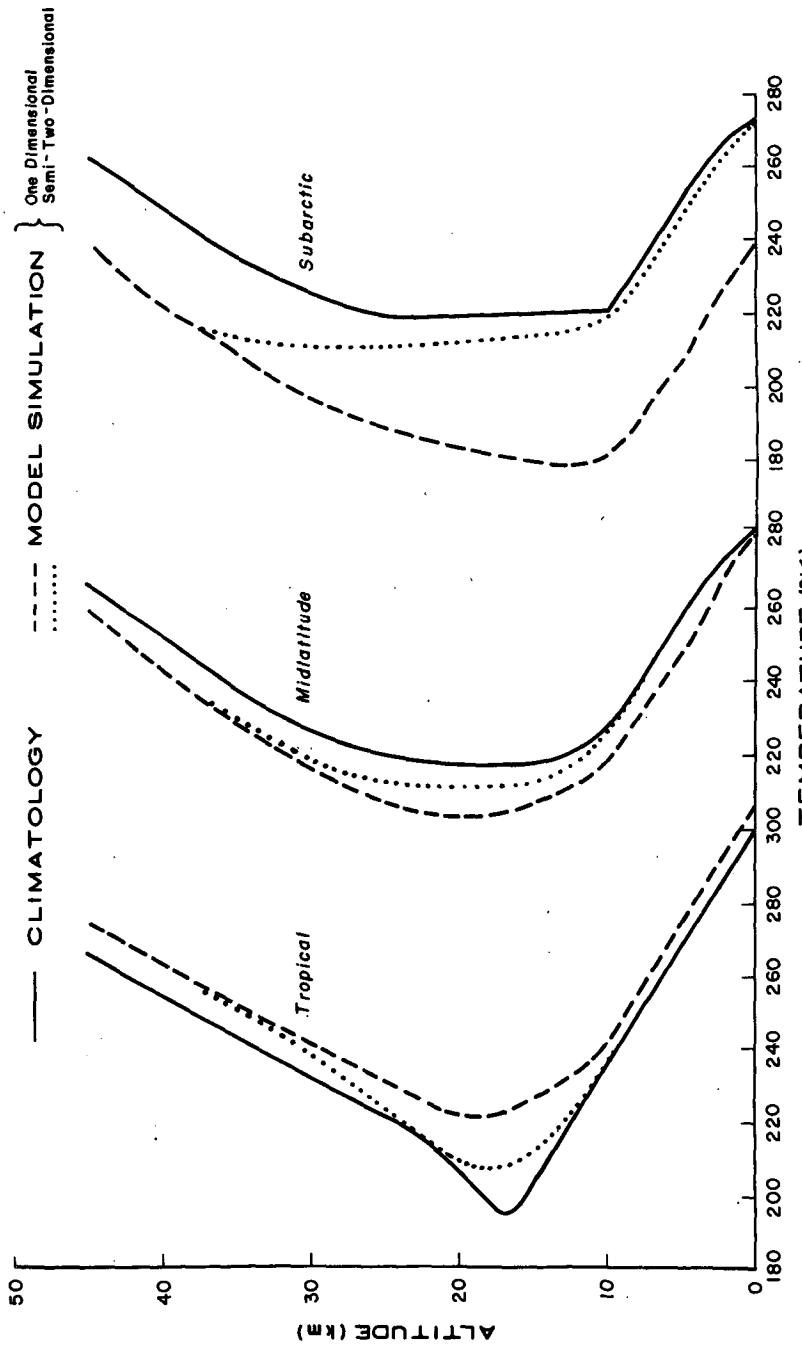

FIG. 8. *Equilibrium temperatures derived from the present one-dimensional (dashed lines) and semi-two-dimensional (dotted lines) models for tropical, midlatitude and subarctic conditions. Solid lines denote climatological temperature profiles.*

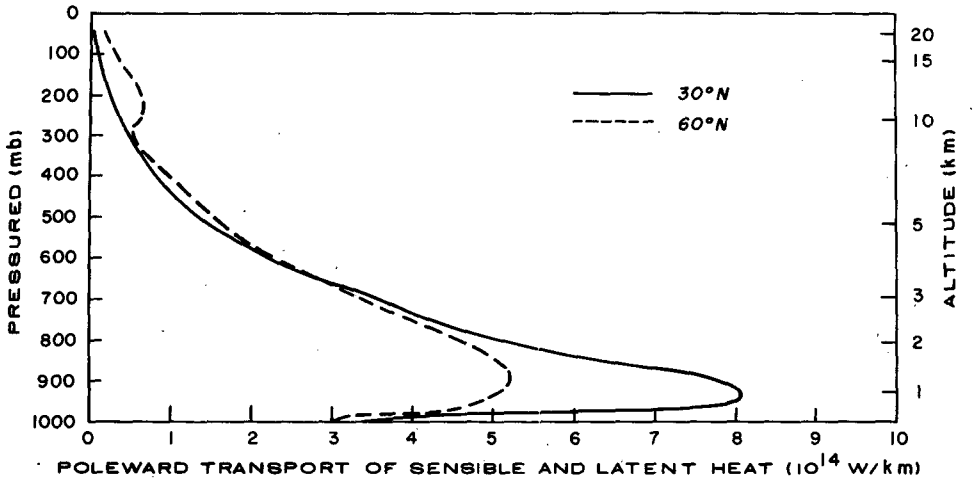

FIG. 9. Poleward transport of sensible and latent heat in units of 10^{14} W km^{-1} at 30 and 60°N computed from the data presented by Oort and Rasmusson (1971).

sphere are a consequence of the large water vapor concentration, small mean solar zenith angle and low surface albedo. On the contrary, however, simulated temperatures for the midlatitude atmosphere (30–60°) and subarctic region (60–90°) are much colder than climatology values. The differences between simulation results and climatology data in the subarctic case are generally greater than 30 K everywhere in the atmosphere. Failure of the one-dimensional radiative-turbulent model to reproduce reliable temperature fields in three latitudinal belts is clearly caused by the neglect of the poleward transport of heat fluxes. Thus, in order to physically simulate temperature fields as functions of both height and latitude, it is necessary to incorporate the horizontal heat transport in the numerical experiment. In conjunction with this, we outline below an empirical-theoretical approach.

b. Semi-two-dimensional model

From the observational data covering a period from May 1958 to April 1963, Oort and Rasmusson (1971) computed the annual mean poleward transport of sensible and latent heat due to the eddy and mean motions as functions of the latitude and height up to 20 km for the Northern Hemisphere. On the basis of their data, we present in Fig. 9 the total transport values at 30 and 60°N taking into account the area involved in these latitudinal zones. The poleward heat transport is in units of 10^{14} W km^{-1}. It is evident that there are positive poleward transports of sensible and latent heat from the tropics to the midlatitude and from the midlatitude to the subarctic region. For the midlatitude region, there is an excess of horizontal heat flux below about 4 km while a deficit takes place above this height. It is anticipated, in view of these transports, that if the horizontal heat flux term in the basic equation shown in Eq. (2.2) is incorporated in the model, simulated temperatures should be improved with reference to climatology data.

To incorporate the horizontal heat transport effect, we consider a steady-state two-dimensional thermodynamic model in the form

$$\frac{1}{a\cos\lambda}\frac{\partial}{\partial\lambda}\cos\lambda F_H(\lambda, z) + \frac{\partial}{\partial z}F_v(\lambda, z) = \frac{\partial}{\partial z}[F_s(\lambda, z) - F_{IR}(\lambda, z)], \quad (5.1)$$

where $F_H(\lambda, z)$ represents the mean and eddy horizontal transports of sensible and latent heat, $F_v(\lambda, z)$, representing the vertical eddy flux, is the first term in Eq. (2.7), a is the radius of the earth and λ denotes the latitude. We perform integration from the surface to a given height to obtain

$$\int_0^z \frac{1}{a\cos\lambda}\frac{\partial}{\partial\lambda}\cos\lambda\, F_H(\lambda, z')dz' = \int_0^z \frac{\partial}{\partial z'}[F_s(\lambda, z') - F_{IR}(\lambda, z') - F_v(\lambda, z')]dz'. \quad (5.2)$$

Upon noting that $F_s(\lambda, 0) - F_{IR}(\lambda, 0) - F_v(\lambda, 0) = 0$, i.e., conservation of radiative and turbulent fluxes at the surface, we find

$$F_v(\lambda, z) + F_{IR}(\lambda, z) = F_s(\lambda, z) - \frac{1}{a\cos\lambda}\frac{\partial}{\partial\lambda}\cos\lambda\int_0^z F_H(\lambda, z')dz'. \quad (5.3)$$

The last term, representing the integrated horizontal heat transport, can be estimated from the data presented by Oort and Rasmusson (1971) for latitudes 30 and 60°. In this manner, while the vertical heat transport is expressed analytically in terms of eddy

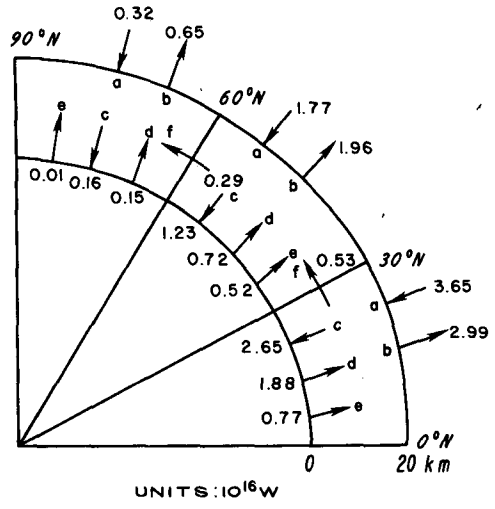

FIG. 10. Two-dimensional heat budget analyses for the tropical, midlatitude and subarctic regions of the Northern Hemisphere. All fluxes are in units of 10^{16} W. (a) Incoming solar net flux at the top, (b) outgoing infrared net flux at the top, (c) incoming solar net flux at the surface, (d) outgoing infrared net flux at the surface, (e) upward eddy flux, (f) poleward horizontal flux.

thermal diffusion processes, horizontal heat transports are also taken into consideration semi-empirically.

In Fig. 8 dots denote the simulation temperatures below 20 km which are adjusted by the horizontal transport utilizing the aforementioned data. Except in the vicinity of the tropopause, the semi-two-dimensional model reproduces reasonable temperature profiles for the tropical and midlatitude regions in reference to the climatology data. Below about 10 km, deviations from the climatological temperatures are within 0.1 K. The simulation temperatures in the subarctic region, however, are still colder than the climatology values by about 5 K. Above 20 km, adjustment of the horizontal transport is not made in equilibrium temperature calculations since no adequate data are available at this time. Thus, in Eq. (5.2) the last term is set to be zero when $z > 20$ km. For all three latitudinal belts, simulated temperature profiles above 20 km gradually approach those computed from the one-dimensional radiative-turbulent model. It is seen that above about 35 km the influence of the radiation emission from the troposphere and lower stratosphere where horizontal heat and dynamic transports are accounted for becomes insignificant. It must be pointed out that simulated temperature profiles above 20 km depicted in the graph are not physically reliable since large-scale horizontal heat transports in the stratosphere are ignored.

In addition, we also wish to point out that in the present semi-two-dimensional model, water vapor transport processes have not been independently treated in the determination of equilibrium temperature. While an interactive water vapor transport program in connection with the one-dimensional model has been proposed by Hummel and Kuhn (1981), a reference cited in the introduction, the incorporation of water budget in a two-dimensional model such as the one presently developed will require appropriate dynamic equations describing the wind field which we try to avoid in the thermodynamic parameterization approach. Certainly, this is one area requiring further research and physical investigations. The present semi-two-dimensional model, however, may be extended to include all the latitudes so that equilibrium temperature profiles as functions of latitude and height may be constructed for both Northern and Southern Hemispheres. To a first approximation we may assume that the horizontal heat transport is independent of the temperature (e.g., if the temperature structure does not change drastically in a perturbation experiment), then we may study the climatic effects of the latitudinal variation of the cloud field including cloud types, positions and compositions on the equilibrium temperature structure. Ultimately, it would be desirable to derive empirically from available data sources the horizontal heat transport as a function of temperature in conjunction with the investigation of the climatic effects of clouds on the thermal structure of the earth-atmosphere system.

Finally, energy budget analyses for the atmospheric column from 0 to 20 km for the Northern Hemisphere derived from the present radiation scheme are depicted in Fig. 10. In the tropics, the net solar and infrared fluxes at the top are 3.65 and 2.99 (all in units of 10^{16} W), respectively. Thus, the gain of the atmosphere is 0.66 units. Based on Vonder Haar and Suomi (1971), the total horizontal heat transport from the tropics to the midlatitude at 30°N is estimated to be 0.53 units. Consequently, the tropical region has a slight energy excess. At the surface, the net solar and infrared fluxes are 2.65 and 1.88 units, respectively. To achieve a balance in a steady-state mode, the upward eddy transport must have a value of 0.77 units. In midlatitudes, there is a deficit of radiation flux in an amount of 0.19 units. However, this baroclinic region has a net gain of the horizontal heat flux of 0.24 units. As a result, there is also a very small energy gain. In the subarctic region, the radiation flux loss and horizontal heat flux gain are, respectively, 0.33 and 0.29 units and therefore there is a small energy deficit. Also note that the vertical eddy transport in this region is very small since the atmosphere is basically stable.

6. Conclusions

An analytic thermodynamic model for the temperature profile determination has been developed on the basis of the balance of radiative and turbulent heat fluxes. In the one-dimensional case, it is illus-

trated that the temperature field is governed by a first-order differential-integro equation using a first-order closure scheme for the vertical eddy thermal flux.

Parameterization of infrared radiative transfer in inhomogeneous atmospheres is carried out utilizing a broadband emissivity approach in which emissivity values for water vapor, carbon dioxide and ozone are fitted in terms of polynomial functions with accuracy within 2%. Moreover, we demonstrate analytically that the net infrared flux at any given atmosphere level is the sum of the Planck fluxes (σT^4) weighted by a proper kernel function which is the slope of the broadband emissivity. For the computation of solar fluxes and heating rates, we develop a parameterization method based on the concept of broadband flux transfer. This allows the separation of absorption due to water vapor, carbon dioxide and ozone and scattering by molecules and cloud particles. Solar heating rates and net fluxes computed from the broadband parameterization scheme are shown to agree well with those derived from a more exact radiative transfer program.

In order to solve for the temperature profile from the first-order differential-integro thermodynamic equation involving temperature to the fourth power under the integral operator, an efficient perturbation scheme is devised for the temperature solution in a radiative-turbulent equilibrium. The technique is based on the perturbation on the deviation of the true temperature from the pure radiative equilibrium temperature utilizing a Taylor series expansion. Numerical experiments reveal that three to four iterations suffice to converge the temperature profiles to within 0.1%. Moreover, we have developed, by virtue of known theories and available experimental data, methods for calculating the eddy thermal diffusion coefficient in various regions of the atmosphere for use in determining radiative-turbulent temperatures. These regions include the constant flux layer, troposphere and stratosphere.

Simulation results in the one-dimensional case using climatological water vapor, ozone and cloud profiles compare closely with the standard temperature profile in the troposphere. Simulated temperatures in the vicinity of the tropopause and the stratosphere deviate from the standard temperature profile within about 5 K. We have also applied the one-dimensional model to tropical, midlatitude and subarctic conditions to quantitatively understand the requirement of the horizontal transport. Resulting temperature profiles show significant deviations from the climatological data with tropics too warm and midlatitude and subarctic regions much too cold. This leads us to introduce a semi-two-dimensional model to account for the horizontal heat transport. By incorporating empirical data for the poleward transport of sensible and latent heat which are available below 20 km, we show that this model reproduces reasonable tropospheric temperatures for the tropical and midlatitude regions as compared with the climatological values. Finally, two-dimensional heat budget analyses using the present radiation programs reveal that there is a slight energy gain and deficit in the tropics and subarctic region, respectively, of the Northern Hemisphere.

Acknowledgments. This research was supported by the Division of the Atmospheric Sciences, National Science Foundation under Grant ATM81-09050 and in part by the Air Force Geophysics Laboratory under Contract F19628-81-K-0042. We thank Ms. Sharon Bennett for typing and editing the manuscript.

REFERENCES

Businger, J. A., J. C. Wyngaard, Y. Izumi and E. F. Bradley, 1971: Flux profile relationships in the atmospheric surface layer. *J. Atmos. Sci.*, **28**, 181–189.

Carrier, G. F., 1974: Perturbation methods. *Handbook of Applied Mathematics*, C. E. Pearson, Ed., Van Nostrand Reinhold, Chap. 14, 761–828.

Charlock, T. P., and W. D. Sellers, 1980: Aerosol effects on climate: Calculations with time-dependent and steady-state radiative convective models. *J. Atmos. Sci.*, **37**, 1327–1341.

Freeman, K. P., and K. N. Liou, 1979: Climatic effects of cirrus clouds. *Advances in Geophysics*, Vol. 21, Academic Press, 231–287.

Gierasch, P., and R. M. Goody, 1968: Study of thermal and dynamical structure on Martian atmosphere. *Planet. Space Sci.*, **16**, 615–644.

Handbook of Geophysics, 1961. Macmillan, Chap. 16.

Howard, J. N., D. L. Burch and D. Williams, 1956: Near-infrared transmission through synthetic atmospheres. *J. Opt. Soc. Amer.*, **46**, 186–190.

Hummel, J. R., and W. R. Kuhn, 1981: An atmospheric radiative-convective model with interactive water vapor transports and cloud development. *Tellus*, **33**, 372–381.

Hunt, B. G., 1981: The maintenance of the zonal mean state of the upper atmosphere as represented in a three-dimensional general circulation model extending to 100 km. *J. Atmos. Sci.*, **38**, 2172–2186.

Inn, E. C., and Y. Tanaka, 1953: Absorption coefficient of ozone in the ultraviolet and visible regions. *J. Opt. Soc. Amer.*, **43**, 870–873.

Katayama, A., 1966: On the radiation budget of the troposphere over the northern hemisphere: I. Introduction. *J. Meteor. Soc. Japan*, **44**, 381–401.

Lacis, A. A., and J. E. Hansen, 1974: A parameterization for the absorption of solar radiation in the earth's atmosphere. *J. Atmos. Sci.*, **31**, 118–133.

Lindzen, R. S., A. Y. Hou and B. F. Farrell, 1982: The role of convective model choice in calculating the climate impact of doubling CO_2. *J. Atmos. Sci.*, **39**, 1189–1205.

Liou, K. N., 1980: *An Introduction to Atmospheric Radiation.* Academic Press, 392 pp.

——, and S. S. Ou, 1981: Parameterization of infrared radiative transfer in cloudy atmospheres. *J. Atmos. Sci.*, **38**, 2707–2716.

——, and K. L. Gebhart, 1982: Numerical experiments on the thermal equilibrium temperature in cirrus cloudy atmospheres. *J. Meteor. Soc. Japan*, **60**, 570–582.

——, and T. Sasamori, 1975: On the transfer of solar radiation in aerosol atmospheres. *J. Atmos. Sci.*, **32**, 2166–2177.

——, and G. D. Wittman, 1979: Parameterization of the radiative properties of clouds. *J. Atmos. Sci.*, **36**, 1261–1273.

London, J., 1957: A study of the atmospheric heat balance. New York University, Final Rept., Contract AF19(122)-166, 99 pp.

Manabe, S., and F. Möller, 1961: On the radiative equilibrium and

heat balance of the atmosphere. *Mon. Wea. Rev.*, **89**, 503–532.

——, and R. Strickler, 1964: Thermal equilibrium of the atmosphere with a convective adjustment. *J. Atmos. Sci.*, **21**, 361–385.

——, and R. T. Wetherald, 1967: Thermal equilibrium of the atmosphere with a given distribution of relative humidity. *J. Atmos. Sci.*, **24**, 241–259.

Oort, A. H., and E. M. Rasmusson, 1971: *Atmospheric Circulation Statistics.* NOAA Prof. Pap. 5, 323 pp. [DOC C 55.25:5].

Priestley, C. H. B., 1959: *Turbulent Transfer in the Lower Atmosphere.* University of Chicago Press, 130 pp.

Ramanathan, V., 1976: Radiative transfer within the earth's atmosphere and stratosphere: A simplified radiative-convective model. *J. Atmos. Sci.*, **33**, 1330–1346.

——, 1981: The role of ocean-atmosphere interactions in the CO_2 climate problem. *J. Atmos. Sci.*, **38**, 918–930.

——, and J. A. Coakley, Jr., 1978: Climate modeling through radiative-convective models. *Rev. Geophys. Space Phys.*, **16**, 465–489.

Reed, R. J., and K. E. German, 1965: A contribution to the problem of stratospheric diffusion by large-scale mixing. *Mon. Wea. Rev.*, **93**, 313–321.

Sarachik, E. S., 1978: Tropical sea surface temperature: An interactive one-dimensional atmosphere-ocean model. *Dyn. Atmos. Oceans*, **2**, 455–469.

Sasamori, T., J. London and D. V. Hoyt, 1972: Radiation budget of the Southern Hemisphere. *Meteor. Monogr.*, No. 35, Amer. Meteor. Soc., 9–23.

Stephens, G. L., and P. J. Webster, 1981: Clouds and climate: Sensitivity of simple systems. *J. Atmos. Sci.*, **38**, 235–247.

Taylor, G. I., 1915: Eddy motion in the atmosphere. *Phil. Trans. Roy. Soc. London*, **A215**, 1–26.

Vigroux, E., 1953: Contributions a l'étude experimentale de absorption de l'ozone. *Ann. Phys.*, **8**, 709–762.

Vonder Haar, T. H., and V. E. Suomi, 1971: Measurements of the earth's radiation budget from satellites during a five-year period. I: Extended time and space means. *J. Atmos. Sci.*, **28**, 305–314.

Wang, W. C., W. B. Rossow, M. S. Yao and M. Wolfson, 1981: Climate sensitivity of one-dimensional radiative-convective models with cloud feedback. *J. Atmos. Sci.*, **38**, 1167–1178.